

Magneto Hydro-Dynamics and Heat Transfer in Liquid Metal Flows

J. S. Rao and Hari Sankar
*Altair Engineering India Pvt. Ltd., Bengaluru, 560103
 India*

1. Introduction

Liquid metals are considered to be the most promising coolants for high temperature applications like nuclear fusion reactors because of the inherent high thermal diffusivity, thermal conductivity and hence excellent heat transfer characteristics. The coolant used in nuclear reactor should have high heat extraction rate. The high melting point and boiling point which eliminates the possibility of local boiling makes liquid metals more attractive to high temperature applications. The thermal entrance length of liquid metals are relatively high leading to flow never reaching fully developed condition which is always advantageous for heat transfer applications as the Nusselt number value is higher in a developing flow than a fully developed flow. The molecular properties of liquid metals are such that the thermal diffusion is faster than momentum diffusion having Prandtl number $\ll 1$. The thermal boundary layer for liquid metal flow is not only confined to the near wall region but also extends to the turbulent core region which makes the turbulent structures important in transfer of heat. As turbulence plays an important role in transfer of heat from the viscous sub-layer to the core flow, it is necessary to maintain high turbulence to achieve high convective heat transfer rates. It may also be noted that surrounding magnetic fields reduce the turbulence and flow becomes more streamlined.

Lithium is the lightest of all metals and has the highest specific heat per unit mass. Lithium is characterized by large thermal conductivity and thermal diffusivity, low viscosity, low vapor pressure as shown in table 1. Lithium is the most promising coolant for thermonuclear power installations. Tritium is a component of fusionable fuel. Tritium does not occur in nature in large amounts and is unstable with its half life 12 years. Tritium can be obtained from lithium with nuclear reactions in fission nuclear reactors or blankets of fusion reactors. Thus, lithium provides raw nuclear fuel to implement fusion reaction.

Density, kg/m ³	Dynamic Viscosity, kg/m-s	Specific Heat, KJ/kg-K	Thermal Conductivity, W/m-K
497	0.0004	4167	50

Table 1. Physical properties of liquid lithium at 650 °C, Davidson (1968)

The plasma generated in the nuclear fusion reactors is confined using an intense magnetic field created by a series of toroidal and poloidal magnets generating magnetic field intensity values of the order 10 Tesla, Kirillov (1994) and is very high compared to the magnetic field

intensity of the earth which is of the order 10^{-4} Tesla, Roberts (1967). The electrical conductivity of liquid metals is of the order 10^6 to 10^7 $1/\Omega\text{-m}$, Davidson (1968). This introduces the term magneto-hydrodynamics relevant to design of liquid metal flows especially in the application as coolant and breeding material in Tritium breeders of nuclear fusion reactors.

Magneto-hydro-dynamics involves study of magnetic fields and fluid flows and their interaction. Alfven (1942) was the first to introduce the term Magneto-hydrodynamics, though Hartmann and Lazarus (1937) earlier performed both theoretical and experimental studies in Magneto-hydrodynamic flows in ducts. Moffatt (1967) showed analytically that the turbulent velocity fluctuation in a flow is suppressed by application of a uniform magnetic field. This chapter is dedicated to the study of how magnetic field affects the convective heat transfer characteristics in liquid metal flows by affecting the following mechanisms.

1. Mean velocity distribution in the flow
2. Velocity fluctuations in time and space

2. The governing equations of magneto-hydrodynamic flows

The hydrodynamic governing equations are the mass (continuity), momentum and energy equations. They are

Continuity equation

$$\frac{\partial \rho}{\partial t} + \nabla \cdot \rho V = 0 \quad (1)$$

where ρ is the density of the fluid and V is the velocity represented by $V = ui + vj + zk$. The first term on the left is the accumulation/unsteady term which can be neglected for steady state condition and second term on the left is mass flux term.

Momentum equation

$$\frac{\partial V}{\partial t} + (V \cdot \nabla)V = -\frac{1}{\rho} \nabla p + \nu \nabla^2 V + S \quad (2)$$

where ν is the kinematic viscosity which is a molecular property of the fluid, p is the pressure. The first term on the left is the unsteady term and the second term on the left is the convection term. The first term on the right is the pressure force term; the second term on the right is the diffusion term which is due to the viscous effects. The third term on the right is the source term which includes other forces such as gravitational forces, electromagnetic forces etc.

Energy equation

$$\rho C_p \left[\frac{\partial T}{\partial t} + (V \cdot \nabla)T \right] = k \nabla^2 T + q''' \quad (3)$$

where k is the thermal conductivity which is a molecular property of the fluid, T is the temperature and C_p is the specific heat of the fluid. The first term on the left is the unsteady term and the second term on the left is the convection term. The first term on the right is the diffusion term. The third term on the right is the source term which includes volumetric heat sources.

The equations given above are generic equations and what differentiates the equation when used for laminar and turbulent flow regimes is the replacement of molecular viscosity, ν and thermal conductivity, k by effective viscosity, ν_{eff} and effective thermal conductivity, k_{eff} in the momentum and energy equation when the flow is turbulent.

$$\nu_{\text{eff}} = \nu_m + \nu_\tau \tag{4}$$

$$k_{\text{eff}} = k_m + k_\tau \tag{5}$$

where ν_τ is the turbulent viscosity which is the increment in momentum transfer due to diffusion created by turbulence and k_τ is the turbulent thermal conductivity which is the increment in heat transfer due to diffusion created by turbulence.

The effect of magnetic field will be included by addition of Lorentz force term $j \times B$ and force due to electric charge $\rho_c E$ as a source term in the momentum equation and inclusion of Joule dissipation term $\frac{j^2}{\sigma}$ as a volumetric heat generation term in the energy equation. The effect of magnetic field on turbulence can be included by altering the turbulent viscosity and turbulent thermal conductivity in the momentum and energy equation respectively. The modified momentum equation including the magnetic effects is given by,

$$\frac{\partial V}{\partial t} + (V \cdot \nabla)V = -\frac{1}{\rho} \nabla p + \nu \nabla^2 V + \frac{1}{\rho} (j \times B) + \frac{1}{\rho} (\rho_c E) + S \tag{6}$$

The modified energy equation including the Joule dissipation is given by,

$$\rho C_p \left(\frac{\partial T}{\partial t} + (V \cdot \nabla)T \right) = k \nabla^2 T + \frac{j^2}{\sigma} + q''' \tag{7}$$

The inclusion of new variables j , E and B in the hydrodynamic equations requires closure equations given using Maxwell's equations

$$\nabla \cdot D = \rho_c \tag{8}$$

$$\frac{\partial B}{\partial t} = -\nabla \times E \tag{9}$$

$$\nabla \cdot B = 0 \tag{10}$$

$$\nabla \times H = j + \frac{\partial D}{\partial t} \tag{11}$$

and Ohms law

$$j = \sigma(E + V \times B) \tag{12}$$

where D is the electric displacement.

The above equations (1), (6)-(12) can be used for a range of problems, but the equations are complex and may not be fully modeled to capture the physics of liquid metal flows and heat transfer.

The Magneto-hydro-dynamic approximation

In applications where the flow velocity is low as compared to the speed of light, the force due to electric charge $\rho_c E$ can be neglected when $U \ll c$ based on

$$\frac{|\rho_c E|}{|j \times B|} \approx \frac{U^2}{c^2} \quad (13)$$

where c is the speed of light. This approximation will eliminate the inclusion of the term $\partial D/\partial t$ from equation (11) and equation (8) can be ignored when $U \ll c$.

Using $B = \mu^* H$ and combining (11) and (12)

$$\frac{1}{\sigma \mu^*} (\nabla \times B) = (E + V \times B) \quad (14)$$

Considering $\nabla \times$ of equation (14) assuming $\eta^* = \frac{1}{\sigma \mu^*}$ is constant, we have

$$\eta^* \{ \nabla (\nabla \cdot B) - \nabla^2 B \} = \nabla \times E + \nabla \times (V \times B) \quad (15)$$

Using (9) and (10), (15) becomes

$$\frac{\partial B}{\partial t} = \nabla \times (V \times B) + \eta^* \nabla^2 B \quad (16)$$

Equation (16) is called the magnetic induction equation; the first term on the right is the induction term and the second term the diffusive term. The induction term describes the interaction of the field with flow. If $Re_m \ll 1$ then the diffusion term is more significant than the induction term and hence the induction equation, for $Re_m \ll 1$ becomes

$$\frac{\partial B}{\partial t} = \eta^* \nabla^2 B \quad (17)$$

$$j = \frac{1}{\mu^*} (\nabla \times B) \quad (18)$$

A summary of equations used for liquid metal flows involving heat transfer in presence of magnetic field is given below namely, mass, momentum, energy and magnetic induction.

$$\frac{\partial \rho}{\partial t} + \nabla \cdot \rho V = 0 \quad (19)$$

$$\frac{\partial V}{\partial t} + (V \cdot \nabla)V = -\frac{1}{\rho} \nabla p + \nu \nabla^2 V + \frac{1}{\rho} \left[\frac{1}{\mu^*} B \cdot \nabla B - \nabla \left(\frac{B^2}{2\mu^*} \right) \right] + S \quad (20)$$

$$\rho C_p \left(\frac{\partial T}{\partial t} + (V \cdot \nabla)T \right) = k \nabla^2 T + \frac{\left(\frac{1}{\mu^*} (\nabla \times B) \right)}{\sigma} + q''' \quad (21)$$

$$\frac{\partial B}{\partial t} = \eta * \nabla^2 B \quad (22)$$

The total number of unknowns is 9 including three scalars of velocity, three scalars of magnetic field, pressure, density and temperature and the number of equations is 8 including continuity, 3 momentum equations, energy and 3 induction equations. We need a closure equation for the set of equations. If the flow is incompressible then we can treat density as constant and hence removing the need of an extra equation. If the flow is compressible then we can use an equation for pressure as a function of temperature and density i.e., $p = f(T, \rho)$ for example like ideal gas law for gases.

3. Non-dimensional numbers

Reynolds Number: The non-dimensional number that gives the ratio of the inertial forces to the viscous forces is Reynolds number defined by

$$\text{Re} = \frac{\text{Inertial Forces}}{\text{Viscous Forces}} = \frac{\rho U_0 L}{\mu}$$

where ρ is the density of the fluid (kg/m^3), L is the characteristic length (m), U_0 is the velocity (m/s) and μ is the dynamic viscosity of the fluid ($\text{kg}/\text{m}\cdot\text{s}$). For liquid metal flows in fusion reactors, the typical values encountered is of the order 10^4 to 10^5 . The transition from laminar to turbulent flows occurs at $\text{Re} \approx 2300$.

Hartmann Number: The non-dimensional number that gives the ratio of the electromagnetic forces to the viscous forces is Hartmann number defined by

$$\text{Ha} = \left(\frac{\text{Electromagnetic Forces}}{\text{Viscous Forces}} \right)^{\frac{1}{2}} = B_0 L \sqrt{\frac{\sigma}{\nu \rho}}$$

where, B_0 is the magnetic field intensity (Tesla), σ is the electrical conductivity of the fluid ($1/\Omega\text{m}$) and ν is the kinematic viscosity of the fluid (m^2/s^2). For liquid metal flows in fusion reactors, the typical values encountered for Ha are of the order 2×10^4 and the effect of viscosity and turbulence on the flow is negligible in those situations.

Stuart Number: The non-dimensional number that gives the ratio of the electromagnetic forces to the inertia forces is Stuart number (also called Interaction Parameter N).

$$\text{N} \equiv \text{St} = \frac{\text{Ha}^2}{\text{Re}} = \frac{\text{Electromagnetic Forces}}{\text{Inertial Forces}} = \frac{\sigma B_0^2 L}{\rho U_0}$$

Stuart number can be used to characterize the effect of magnetic field on turbulence as it represents the ratio of large-eddy turnover time τ to the Joule time τ_m . Stuart number shows the ability of the magnetic field to change the isotropic turbulent structures to anisotropic two-dimensional turbulence. When N is small, the anisotropy induced by Joule dissipation is negligible and when it is larger than a critical value N_c , Lorentz force will drive turbulence to two-dimensional situation. The significance of St is found in recent days as the transition of turbulent flow will happen in the range 10^1 to 10^2 as reported by Uda *et al.* (2001) and a sudden increase of turbulence is noted to happen at Stuart number equal to 10. Another

interpretation of Stuart number can be that when N is small, the electromagnetic forces will be weak and will not be able to affect the flow.

Magnetic Reynolds Number: The non-dimensional number that gives the ratio of the momentum diffusivity to the electromagnetic diffusivity defined by

$$\text{Re}_m = \frac{\text{Momentum Advection}}{\text{Magnetic Diffusion}} = \frac{U_0 L}{\mu^* \sigma}$$

where, μ^* is the fluid magnetic permeability (h/m). It characterizes the effect of induced magnetic field on the resultant magnetic field due to the imposed and induced magnetic fields. At $\text{Re}_m \ll 1$ the imposed magnetic field will guide the flow and will be independent of the induced magnetic field as it will be very small compared to the imposed magnetic field. The Lorentz force will be a linear function of velocity when $\text{Re}_m \ll 1$ and quasi-static approximation can be applied. At $\text{Re}_m \gg 1$ the dependence between the magnetic field and velocity is non-linear as the imposed magnetic field is a function of velocity.

Another interpretation of magnetic Reynolds number is based on the ratio of characteristic time scale of diffusion of magnetic field to the time scale of turbulence defined by

$$\text{Re}_m = \frac{\text{Time scale of diffusion of magnetic field}}{\text{Time scale of turbulence}} = \frac{vL}{\frac{1}{\mu^* \sigma}}$$

where v is the rms fluctuating velocity represented as

$$v = \sqrt{\frac{R_{ij}}{3}} \text{ where } R_{ij} = \overline{u_i u_j}$$

and u_i is the fluctuating velocity. At $\text{Re}_m \ll 1$ the distortion of magnetic field lines by the fluid turbulence is small and the induced magnetic fluctuations with respect to the mean magnetic field is also small.

Batchelor number (Magnetic Prandtl Number): The non-dimensional number that gives the ratio of the momentum diffusivity to the electromagnetic diffusivity is Batchelor number defined by

$$\text{Bt} \equiv \text{Pr}_m = \frac{(\text{Viscous diffusion length})^2}{(\text{Electro-magnetic diffusion length})^2} = \frac{\nu}{\nu_m} = \mu^* \sigma \nu$$

It characterizes the ratio of thickness of hydrodynamic boundary layer to magneto-hydrodynamic layers. For liquid metal flows typical values encountered are of the order of 10^{-5} to 10^{-7} . When Pr_m is small, the effect of an external magnetic field is known to be stabilizing and weakly dependent on Pr_m in a variety of flow configurations.

4. Effect of MHD on mean velocity distribution in duct flows

Many analytical studies have been conducted in fully developed duct flows starting from 1930 onwards with some significant contributions by Hartmann (1937), Shercliff (1953) and Hunt (1965). Most of the analytical studies are performed on rectangular cross-section

because of the ease of assigning the direction of the magnetic field and also due to the ease of non-dimensionalizing the MHD equations over the channel height and width. An axial magnetic field does not have much significance in redistribution of mean velocities in duct flow whereas a transverse magnetic field significantly influences the mean velocity distribution. This is because the value of the Lorentz force acting on the body is not significant for a flow subjected to an axial magnetic field Kirillov (1994) as shown in figure 1, because the net Lorentz force is zero (the cross product of two vectors in the same direction is zero). Studies have shown that a transverse magnetic field affects the mean velocity distribution near the walls based on the distribution of induced currents in the duct cross-section depending on the electrical conductivity of the duct walls. The direction of the Lorentz force will act against the flow direction as per right hand thumb rule.

Classical analytical studies with transverse magnetic fields showed that for $Ha \gg 1$ there exist exact solutions for the governing equations or solutions in the form of infinite series as shown in Hartmann (1937), Shercliff (1953) and Hunt (1965). It was found that there exists a core region in the flow where the pressure forces are balanced by the Lorentz force and velocity is uniform in the region. Special boundary layers exist depending on the orientation of the wall with respect to the magnetic field.

Hartmann Layer: Hartmann layer refers to the thin boundary layers formed near the walls perpendicular to the magnetic field and hence has a normal magnetic field. The thickness of the Hartmann layer is of the order $O(Ha^{-1})$ and the viscous forces balance with the magnetic forces in the Hartmann layer. Hartmann layers have a major influence on the core region when the electrical conductivity of the Hartmann walls is low, Fink and Beaty (1999).

Shercliff/Shear/Side Layers: The boundary layers formed on the walls parallel to the magnetic field (side walls) can have different characteristics based on the electrical conductivity of the walls. The layers can either stay near the walls or exist some distance away from the wall in the form of shear layers. The thickness of the boundary layers formed on the side wall is of the order $O(Ha^{-1/2})$ and is higher than that of Hartmann layers. The boundary layers formed near the side walls influence the core region significantly only if the Hartmann walls are electrically conducting and the side walls are insulating, Fink and Beaty (1999).

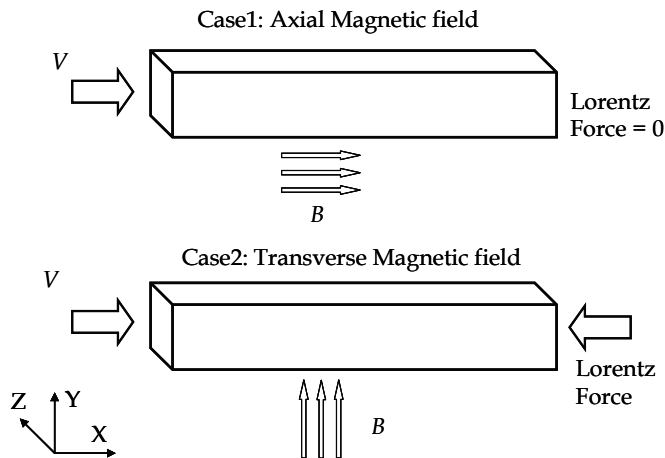


Fig. 1. Schematic showing the direction of Lorentz Force

The schematic of the cross-section of a rectangular duct used for the analytical studies is shown in figure 2. The direction of flow is along the z coordinate and the external magnetic field B_0 is applied in the y direction. The walls BB are the Hartmann walls as they are perpendicular to the magnetic field and walls AA are the side walls as they are parallel to the magnetic field. The dimensions of the duct in x and y directions are $2a$ and $2b$ respectively. The dimensions of the duct are non-dimensionalized as $\eta = y/a$ and $\xi = x/b$.

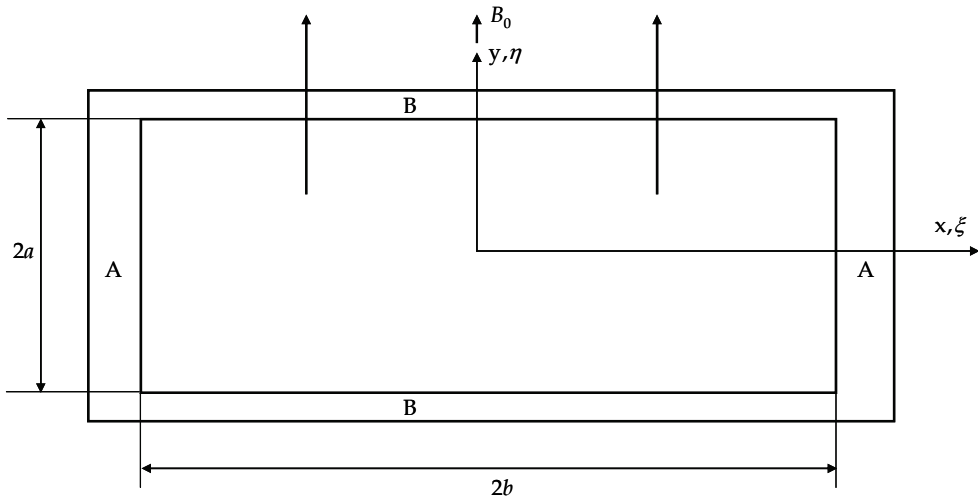


Fig. 2. Schematic of rectangular duct with magnetic field applied in y direction

4.1 Mean velocity distribution parallel to magnetic field (Hartmann layers)

The significance of Hartmann layer on the flow depends on the electrical conductivity of the walls. If the electrical conductivity of the Hartmann walls is low (insulating), then the currents induced in the core regions close in the Hartmann layers and hence making it important in deciding the resistance offered by magnetic field on the flow. If the Hartmann walls are electrically conducting, then the electric current lines close in the walls and hence the significance of the Hartmann layer on the flow reduces. The mean velocity distribution perpendicular to the Hartmann wall is given using the relation given by Hartmann (1937). The thickness of Hartmann layer is proportional to Ha^{-1} . The normalized axial velocity perpendicular to the Hartmann wall is solved analytically by Hartmann (1937) for a duct having insulating Hartmann walls.

$$\frac{U}{U_c} = \frac{Ha}{Ha - \tanh(Ha)} \left[1 - \frac{\cosh(Ha\eta)}{\cosh(Ha)} \right] \quad (23)$$

If Ha grows, the velocity profile becomes more and more flattened as shown in figure 3. This effect is known as the *Hartmann effect*. The thin layer near the wall where the flow velocity changes from zero to U_c is called the *Hartmann layer*. The Hartmann effect is caused by the Lorentz force, which accelerates the fluid in the Hartmann layers and slows it down in the bulk. The case of Hartmann walls having high electrical conductivity is given by Hunt and

Stewartson (1965) and is similar to that of the solution shown in figure 3. This states that the Hartmann layer velocity profile is independent of the electrical conductivity of the Hartmann walls but its control on the core flow will be high if the electrical conductivity of the Hartmann walls is high because the electric field will be stronger.

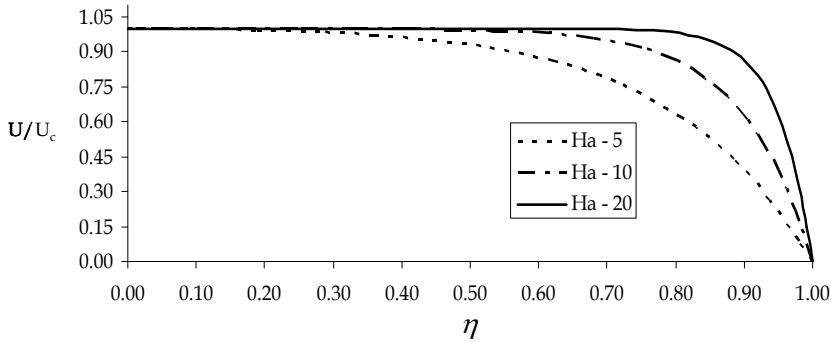


Fig. 3. Normalized axial velocity profiles in the Hartmann layer (centre of duct)

4.2 Mean velocity distribution perpendicular to magnetic field (side layers)

The mean velocity distribution depends on the distribution of electric current lines in the duct which depends on the electrical conductivity of the duct walls. The side layer thickness varies as a function of $Ha^{-1/2}$. Different cases based on the electrical conductivity of walls AA and BB, denoted by d_A and d_B respectively is given in sections 4.2.1 to 4.2.4.

4.2.1 Case 1: Rectangular duct with $d_B = 0, d_A = 0$

The mean velocity distribution perpendicular to the side wall for a rectangular duct with all walls electrically insulating is given using the relation Shercliff (1953) and then developed by Muller and Buhler (2001) as given by equation (24).

$$U \approx \sum_{i=1,3,5}^{\infty} u_i(y) \cos(\lambda_i x) \tag{24}$$

$$u_i(y) = \frac{k_i}{\lambda_i^2} \left\{ 1 - \frac{f_i(y)}{f_i(1)} \right\}$$

$$f_i(y) = \alpha_{i2} \cosh(p_{i1}y) - \alpha_{i1} \cosh(p_{i2}y)$$

$$\lambda_i = \frac{i\pi}{2d}$$

$$k_i \equiv \frac{2 \sin(\lambda_i d)}{\lambda_i d}$$

$$\gamma \equiv \sqrt{Ha^2 + 4\lambda_i^2}$$

$$p_{i1,2} = \frac{1}{2}(\text{Ha} \mp \gamma)$$

$$\alpha_{i1,2} = \sinh(p_{i1,2})$$

The normalized axial velocity with respect to the normalized distance ξ from the side walls is plotted for various Hartmann numbers as shown in figure 4.

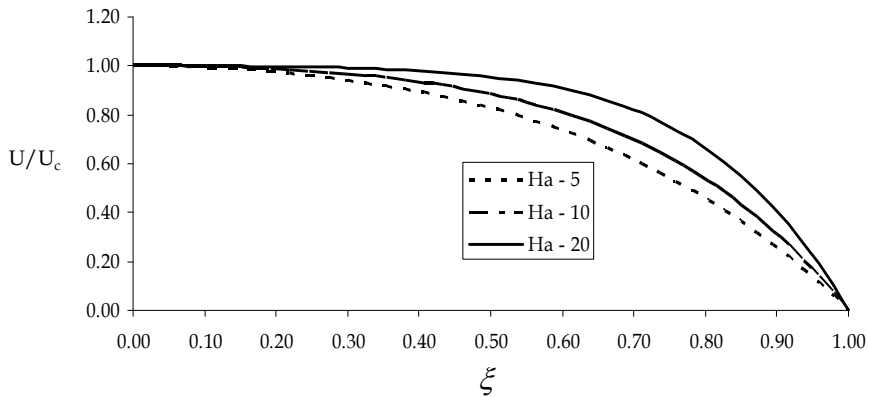


Fig. 4. Normalized axial velocity profiles in the side wall boundary layer

4.2.2 Case 2: Rectangular duct with $d_B = 0$, $d_A = \infty$

The mean velocity distribution perpendicular to the side wall for a rectangular duct with Hartmann walls electrically insulating and electrically conducting side walls is given by Hunt and Stewartson (1965). The axial velocity normalized with respect to the core velocity plotted against the $\text{Ha}^{1/2}(b - \xi)$ is shown in figure 5. It can be seen that the velocity profile is similar to case 1 i.e. Rectangular duct with $d_B=0$, $d_A=0$. This states that when the Hartmann walls are electrically insulating then the velocity profile near the side walls is independent of the electrical conductivity of the side walls.

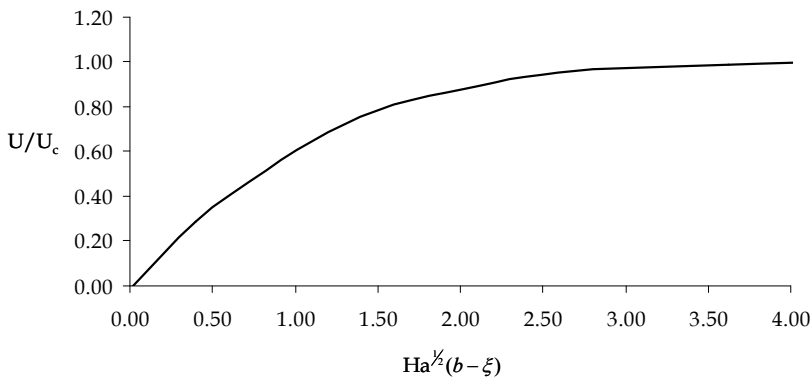


Fig. 5. Normalized axial velocity profiles in the side wall boundary layer

4.2.3 Case 3: Rectangular duct with $d_B = \infty, d_A = 0$

The mean velocity distribution perpendicular to the side wall for a rectangular duct with all walls electrically conducting is given by Hunt (1965). The mean velocity distribution perpendicular to the side wall is given using the relation Hunt (1965) as $Ha \rightarrow \infty$

$$U \approx \sum_{j=0}^{\infty} \frac{2(-1)^j \cos \alpha_j \eta}{Ha^2 \alpha_j} \left[1 - \exp(-\lambda_j \xi) \left\{ \cos(\lambda_j \xi) - \frac{Ha}{\alpha_j} \sin(\lambda_j \xi) \right\} \right] \tag{25}$$

$$\alpha_j \approx \left(j + \frac{1}{2} \right) \pi$$

$$\lambda_j \approx \left(\frac{1}{2} \alpha_j Ha \right)^{\frac{1}{2}}$$

The axial velocity normalized with respect to the normalized distance from the side walls is plotted for various Hartmann numbers as shown in figure 6. The maximum velocity in the side layers is of the order $O(Ha)V_c$ and the maximum velocity on the side wall jet tends to $0.25HaV_c$ as $Ha \rightarrow \infty$, while the minimum velocity becomes locally negative for $Ha > 89$ and tends to $-0.011 HaV_c$. The high velocity gradients near the side walls generate instabilities at high Hartmann numbers. The high velocity jets formed near the side walls results in velocity deficit in the core region and in the Hartmann layers.

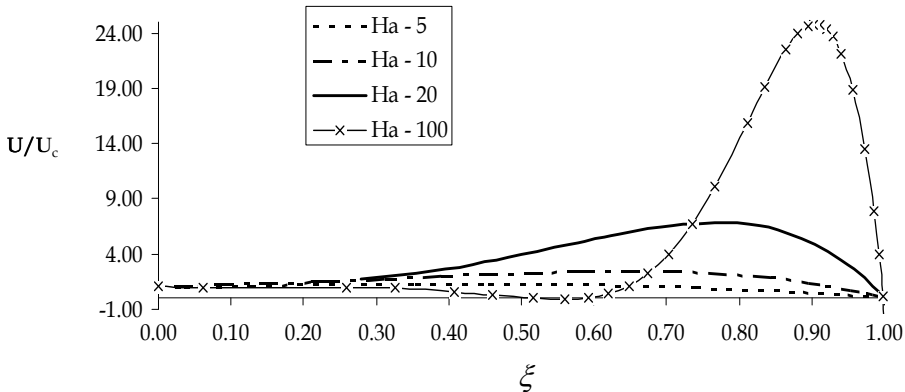


Fig. 6. Normalized axial velocity profiles in the side wall boundary layer

4.2.4 Case 4: Rectangular duct with $d_B = \infty, d_A = \infty$

The mean velocity distribution perpendicular to the side wall is given using the relation given by Hunt (1965). The maximum velocities in the boundary layer are higher than the core velocity but are of the same order unlike the case with $d_A = 0$

$$U \approx \sum_{j=0}^{\infty} \frac{2(-1)^j \cos \alpha_j \eta}{Ha^2 \alpha_j} \left[1 - \exp(-\lambda_j \xi) \left\{ \cos(\lambda_j \xi) - \sin(\lambda_j \xi) \right\} \right] \tag{26}$$

The axial velocity normalized with respect to the normalized distance from the side walls is plotted for various Hartmann numbers as shown in figure 7. The velocity near the side wall increases with increase in magnetic field, but the maximum value of velocity jets approaches $1.25V_c$ when $Ha \rightarrow \infty$.

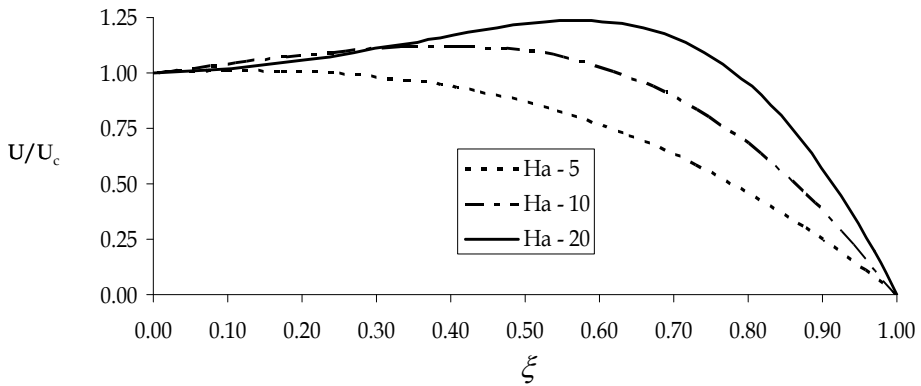


Fig. 7. Normalized axial velocity profiles in the side wall boundary layer

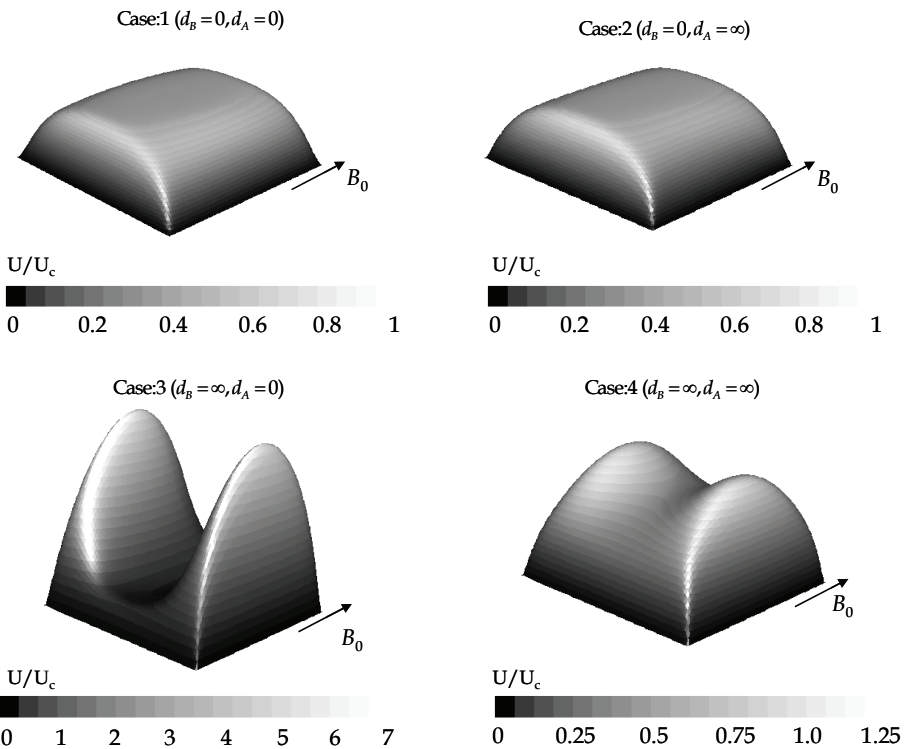


Fig. 8. Axial velocity normalized with respect to the core velocity plotted for $Ha = 20$

4.3 Comparison on mean axial velocity profiles

The analytical solutions of the mean velocity distribution presented in the previous sections are supported using numerical simulations performed for laminar ($Re \approx 10$) steady state flow of an electrically conducting fluid in a square duct using FLUENT (version 6.3.26), see figure 8. The velocity profile near the Hartmann walls is independent of the electrical conductivity of the walls as stated in section 4.1 and the velocity gradients and thickness seems to be similar. The velocity profiles near the side walls shows different characteristics depending on the electrical conductivity of the walls. The velocity profiles for case 1 in section 4.2.1 and case 2 in section 4.2.2 are similar as the induced field has low strength due to the high resistance offered by the Hartmann walls.

In the cases where $d_B = 0$ the net electrical current in the circuit will be low and current lines will not be strong enough to create a redistribution in the mean velocity field as shown in figure 8 and the imbalance between the Lorentz forces and pressure will not be significantly high.

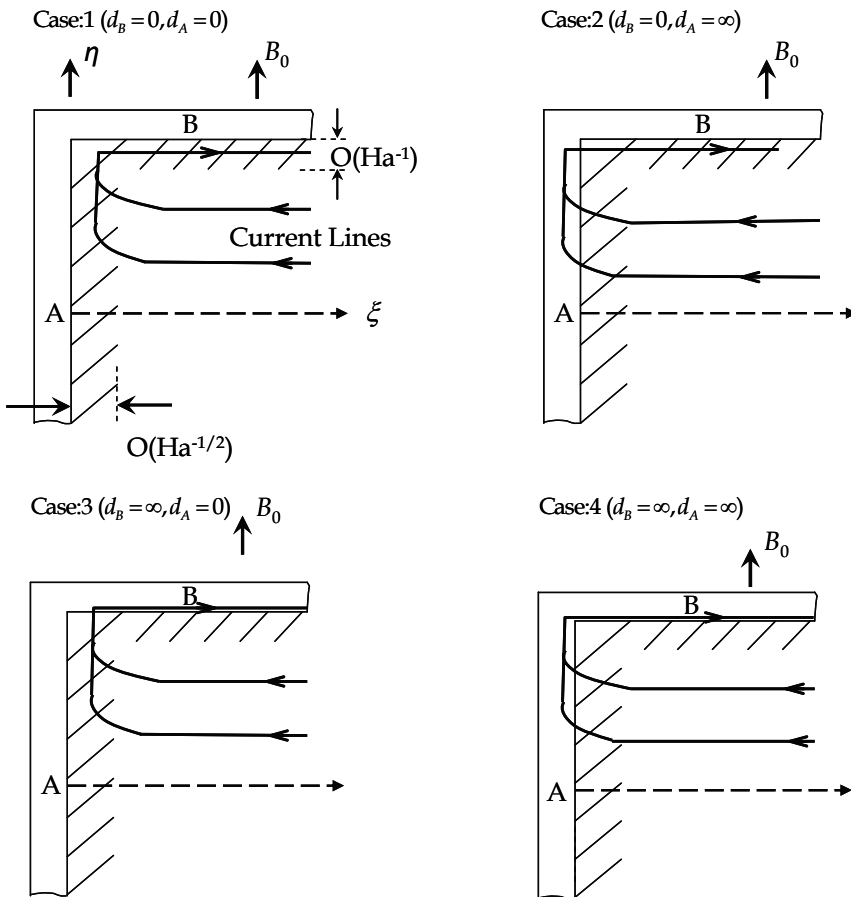


Fig. 9. Schematic of the current lines in the rectangular duct

The distribution of induced current lines in the cross section for different cases is given in figure 9. The formation of shear layers in the case 3 given in section 4.2.3 where $d_B = \infty$ and $d_A = 0$ is due to the imbalance in the Lorentz forces and pressure forces. If $d_A Ha^{1/2} \ll 1$, then the current lines return to walls BB through boundary layers on wall AA and hence the Lorentz force term drops near the boundary layer as compared to other regions making the velocity near the side walls to shoot up as shown in figure 9.

If $d_A Ha^{1/2} \gg 1$ then the current lines returns to wall BB through walls AA which makes the induced magnetic field and hence the Lorentz Force ($j \times B$) term uniform in the duct cross-section which happens in case 4 of section 4.2.4 shown in figure 8 and figure 9. Higher the value of electrical conductivity of side walls, lower the value of the maximum velocity of the jet for case 3 and case 4.

5. Effect of MHD on turbulence suppression

An external magnetic field suppresses the turbulent fluctuations in liquid metals (Low magnetic Prandtl number fluid) independent of the direction of magnetic field with respect to the flow and independent of the mean velocity distribution in the flow. The flow regimes in magneto-hydrodynamic flows of liquid metals, i.e. $R_m \ll 1$, see Fink and Beaty (1989) is shown in figure 10. It can be seen that the flow regime above line 'A' is the laminar regime.

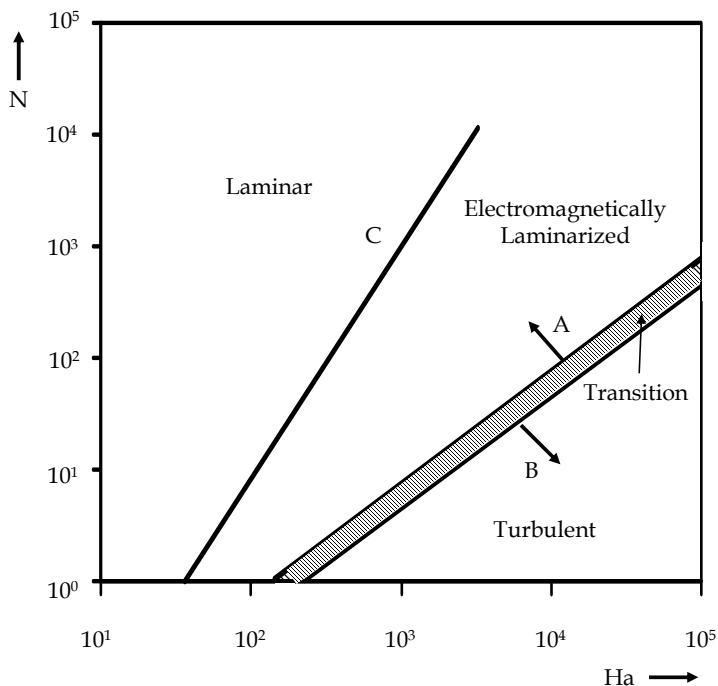


Fig. 10. Turbulent flow regimes in low magnetic Reynolds number flows, Fink and Beaty (1989)

The flow regime below line 'B' is turbulent regime with low values of Stuart number N , in which the influence of the magnetic field on the flow is less. The shaded region between line 'A' and line 'B' is the transition region in which the turbulence levels increase and will be greater than the flow without magnetic field as stated in Uda *et al.* (2001 and 2002). The line 'C' in figure 10 represents the critical Reynolds number for laminar to turbulent transition equal to 2000. The region on the left side of line 'C' is the classical laminar flow regime. The region on the right side of line 'C' and above line 'A' is the region of electromagnetically laminarized flow in which the turbulent flow is converted to so-called Stokes flow in which the inertial term is negligible as mentioned in Happel (1981).

Axial magnetic field suppresses turbulent fluctuations and also increases the critical Reynolds number for transition from laminar to turbulent regime as stated in Kirillov (1994). A transverse magnetic field also has the effect of turbulence reduction. Moffat (1967). The turbulent structures get aligned with the magnetic field lines. As shown in figure 11, when the magnetic field increases, the MHD effect suppresses the turbulence significantly and the large vortex structure breaks up into several small vortex structures. At the same time, the vortex structure was dampened and stretches along the flow direction (perpendicular to the magnetic field).

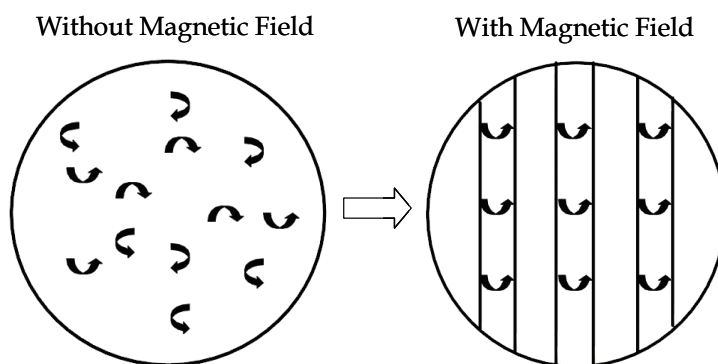


Fig. 11. Change of isotropic turbulent structures to anisotropic structures, Luo *et al.* (2003)

6. Effects of mean velocity distribution and turbulence suppression on convective heat transfer

The convective heat transfer characteristic is affected by magnetic field due to two main mechanisms. Evtushenko (1995)

1. Mean velocity distribution in the flow
2. Velocity fluctuations in time and space

The first mechanism, mean velocity distribution has to take into account two important factors: (1a) the increase of velocity and velocity gradients near side walls parallel to the magnetic field and (1b) Velocity (flow rate) redistribution in the magnetic field direction. The second mechanism, effect of MHD on turbulent fluctuations and hence heat transfer has to take into account important factors like (2a) Damping of turbulent fluctuations, (2b) transition to two-dimensional structure and (2c) the instabilities created in the high velocity jets near the side wall.

6.1 Effect of axial magnetic field on convective heat transfer

In case of flow of liquid metals in heated channels under the influence of a uniform axial magnetic field shows a decrease of convective heat transfer at low and moderate Hartmann numbers whereas the convective heat transfer and hence Nu increases at higher Hartmann numbers as shown in Miyazaki (1988). It was stated in section 4 that an axial magnetic field does not affect the mean velocity distribution so the modification of convective heat transfer is due the variation in the turbulent fluctuations in time and space.

Reynolds number	Hartmann Number	Nu/Nu _{$\beta=0$}
$(2.5 - 5) \cdot 10^3$	360	0.83
$(1 - 2) \cdot 10^4$	700	0.50
$(3 - 4) \cdot 10^4$	1400	0.30
$1 \cdot 10^4$	3600	2.75

Table 2. Variation of Nusselt Number with Axial Magnetic Field, Miyazaki (1988)

The values of Nu for various value of Hartmann numbers is shown in table 2. It can be seen that the values of Nu decreases from its value, $Nu/Nu_{\beta=0} = 1$, at $Ha = 0$. The decrease in Nu value for small and moderate Ha is more when the Reynolds number is high because of the higher turbulence content in the flow. At lower values of Reynolds numbers, the flow will be inherently laminar and therefore the reduction in Nu due to suppression of turbulent fluctuations will be low.

At high values of Hartmann numbers, the Nusselt number was found to increase, violating the earlier theories and studies, see Miyazaki (1988). Miyazaki attributes the increase in the Nusselt number is due to the increase in turbulence levels in the flow as the effect of buoyancy can be ruled out because the flow direction upwards.

6.2 Effect of transverse magnetic field on convective heat transfer

The studies in the field of effect of magnetic field on convective heat transfer in ducts subjected to transverse magnetic field can be classified into two cases

1. Absence of high velocity jets near the side walls
2. Presence of high velocity jets near the side walls

6.2.1 Case 1: Absence of high velocity jets near the side walls

In case of ducts having Hartmann walls with zero conductivity, high velocity jets will not be formed near the side walls. Gardener and Lykoudis (1971b) performed experiments with flow of Mercury in horizontal electrically insulated pipe subjected to transverse magnetic field. It was found that the velocity profile near the Hartmann wall becomes flat with increase in magnetic field as discussed in section 4.1 and the velocity profile near side walls becomes round as discussed in sections 4.2.1 and 4.2.2. The mean velocity distribution is not much different with the increase in magnetic field, so the modification of turbulence phenomenon by the magnetic field will affect the convective heat transfer predominantly for this case. The Nusselt number distribution near the Hartmann and side walls for a range of Reynolds numbers and Hartmann numbers is shown in figure 12. The decrease of Nusselt number with increase in magnetic field is lesser at lower Reynolds number because the turbulence content in the flow at low Reynolds number will be lesser.

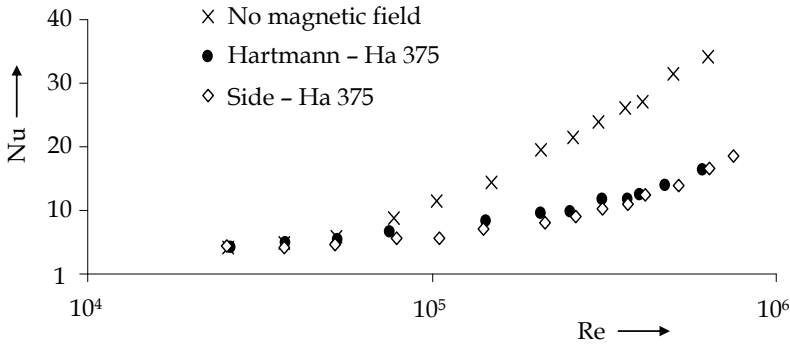


Fig. 12. Nusselt number with magnetic field intensity, Gardener and Lykoudis (1971b)

The reduction in Nusselt number with increase in magnetic field is because of the reduction in turbulence quantified using turbulence kinetic energy as shown in figure 13. It was found that the turbulent kinetic energy decreases both near the Hartmann and side walls with increase in magnetic field where $r/R = 0$ represents the centre of the duct and $r/R = 1$ represents the walls. The damping force within the Hartmann layer is much higher than at the side region due to the high local electric current density. The turbulence in core is suppressed initially and then the turbulence in the Hartmann layer followed by the turbulence near the side wall.

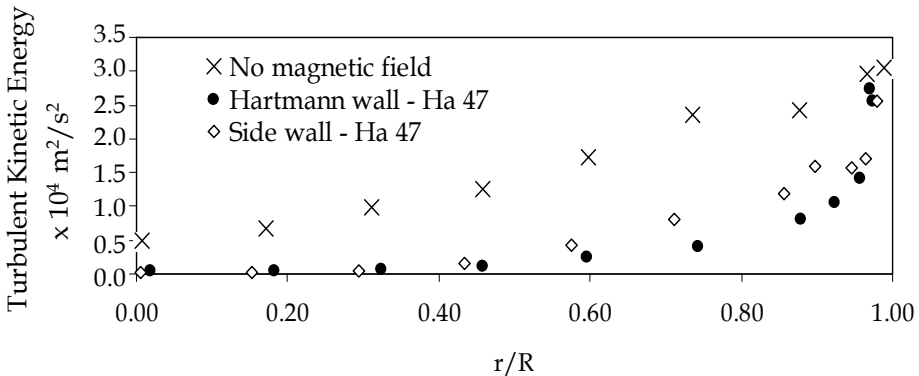


Fig. 13. Turbulent kinetic energy vs. r/R for $Re = 50,000$, Gardener and Lykoudis (1971a)

A correlation for Nusselt number values is created from various experimental results by Ji and Gardener (1997) and is given using the following relation as a function of Peclet number Pe and Hartmann number Ha

$$Nu = 7 + \frac{0.00782Pe^{0.811}}{(1 + 0.0004Ha^{1.5}f(Pe))} \tag{27}$$

$$f(Pe) = (0.3 + 4.75 \times 10^{-5}Pe - 2.10 \times 10^{-9}Pe^2)$$

6.2.2 Case 2: Presence of high velocity jets near the side walls

In case of ducts having Hartmann walls with finite conductivity, high velocity jets will be formed near the side walls. The side layers with high velocity jets (M shaped profile, figure 8 case 3) carry high mass flux is the prime reason for increase of heat transfer near the side walls. Miyazaki et al. (1986) performed experiments to determine the heat transfer characteristics for liquid metal Lithium flow in annular duct with electrically conducting walls under the influence of transverse magnetic fields. The Nusselt number plotted with magnetic field is shown in figure 14. It can be seen that the Nusselt number increases near the side walls and decreases near the Hartmann walls. A singular rise of Nusselt number can be seen near both the walls.

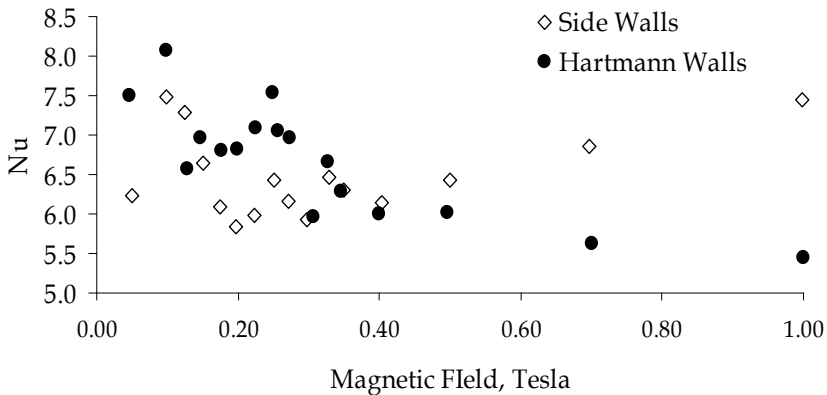


Fig. 14. Nusselt number plotted with magnetic field intensity, Miyazaki (1986)

This effect of heat transfer enhancement near the side walls is caused by the generation and development of large scale velocity fluctuations in the near wall area. The reduction in Nusselt number near the Hartmann walls is created due to the turbulence reduction as shown in figure 15.

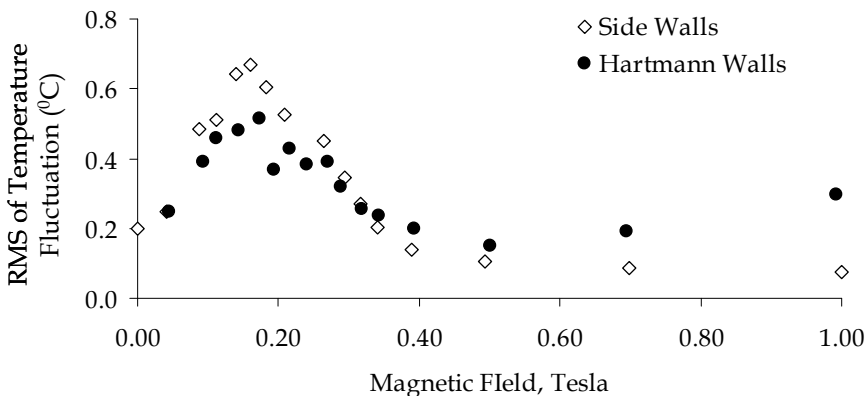


Fig. 15. RMS of temperature fluctuation with magnetic field intensity, Miyazaki (1986)

7. Application of numerical codes

A difficulty in experimental study of the flow of liquid metals arises as the visualization is not possible because of the opaque nature of liquid metals. Application of closed form analytical solutions is limited to simple cases where the equations are not very complex. This makes the application of numerical simulations useful for the study of liquid metal magneto-hydro-dynamic flows. An example of application of a numerical code to explain the mechanisms affecting heat transfer for flow subjected to transverse magnetic field is explained using a series of simulations given in Rao and Sankar (2010), see figure 16.

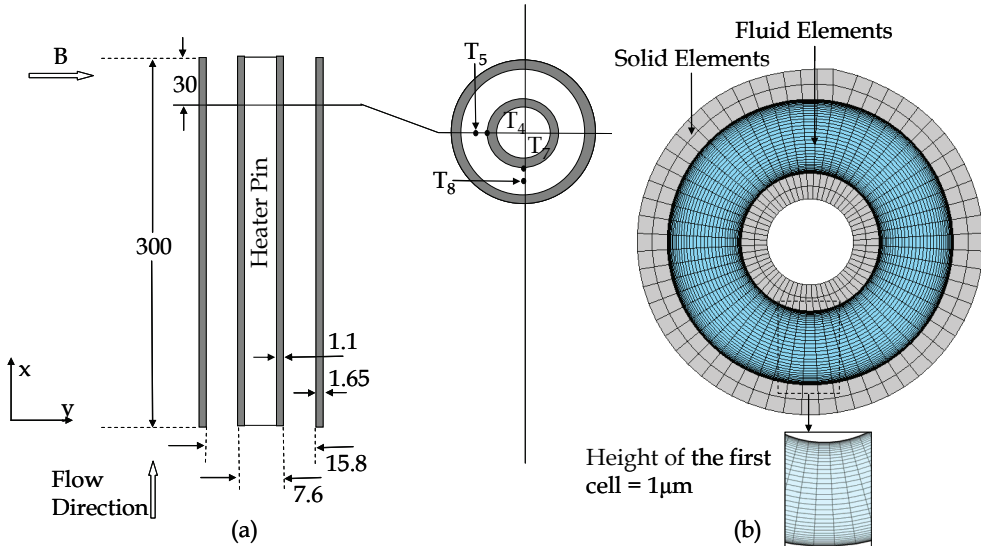


Fig. 16. (a) Schematic of model (b) Details of the computational mesh, Rao and Sankar (2010)

A numerical study is conducted in an annular duct formed by a SS316 circular tube with electrically conducting walls and a coaxial heater pin, with liquid Lithium as the working fluid for magnetic field ranging from 0 - 1 Tesla. The Hartmann and Stuart number of the study ranges from 0 - 700 and 0 - 50 respectively. The Reynolds number of the study is 10^4 . It was shown that the convective heat transfer and hence the Nusselt number decreases near the walls perpendicular to the magnetic field due to reduction in turbulent fluctuations with increase of magnetic field. It was observed that the Nusselt number value increases near the walls parallel to the magnetic field as the mean velocity increases near the walls. A singular rise was observed near both the walls near Stuart number ~ 10 which is due to the increase of turbulence levels in the process of changing from turbulent to electromagnetically laminarized flow, see figure 17.

When a very low Reynolds number ~ 300 is used, the reduction in Nusselt number near the Hartmann walls is less as shown in figure 18. This shows that the reduction in Nusselt number near the Hartmann walls for the high Reynolds number study is due to the reduction in turbulent fluctuations. The Nusselt number was found to increase near the side walls as the mean velocity increases near the walls. When an insulating duct is used the Nusselt number near the parallel walls did not increase for the case with insulating walls as

in the case with conducting walls showing the contribution of the 'M' shaped velocity profile in the Nusselt number increase near the parallel walls. The Nusselt number near the perpendicular walls was found to decrease at a higher rate in case of insulating walls than that of the study with conducting walls as shown in figure 19.

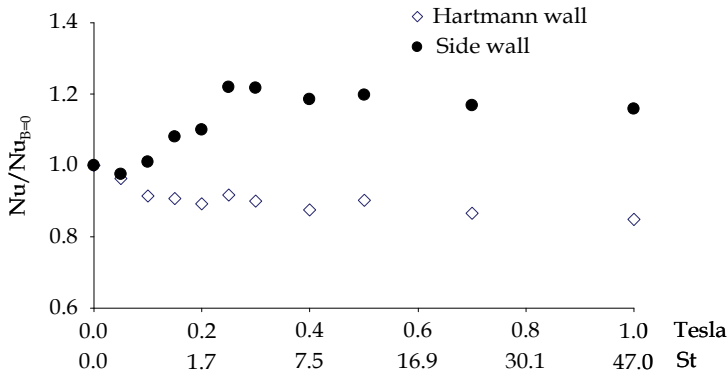


Fig. 17. High Reynolds number with conducting walls, Rao and Sankar (2010)

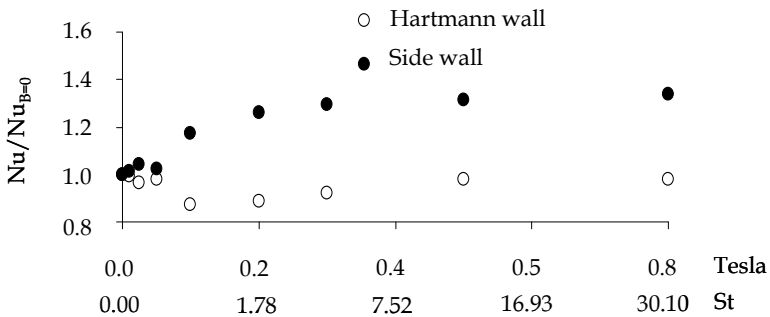


Fig. 18. Low Reynolds number with conducting walls, Rao and Sankar (2010)

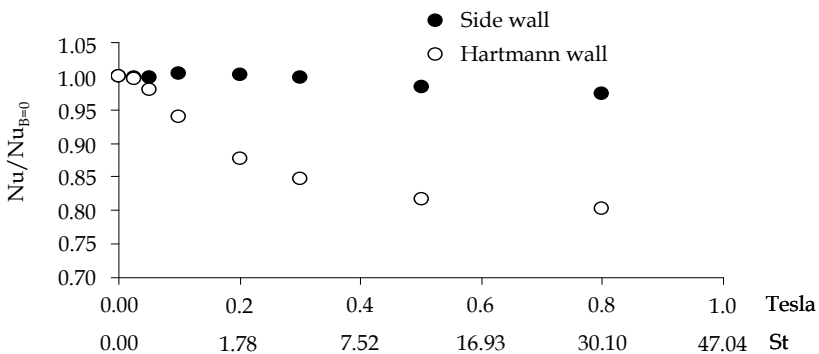


Fig. 19. High Reynolds number with insulating walls, Rao and Sankar (2010)

8. Application of liquid metal MHD studies in nuclear fusion reactors

International Thermo-nuclear Experimental Reactor is an international organization formed in 1985 comprising of researchers from US, EU, China, Japan, India, Korea and Russia working towards development of a test reactor (TOKOMAK) which is expected to be developed by 2020. The test reactor will be installed in France where the head office of ITER is situated. Salient details of the reactor to be developed are shown in figure 20. The reactor height will be close to 100 ft and would weigh around 38000 tons. The cryostat is the external chamber around the TOKOMAK which maintains high vacuum inside it to reduce the heat load from atmosphere through conduction and convection. The fusion of Deuterium and Tritium happens inside the plasma chamber. The magnets are used to confine the plasma created inside the plasma chamber using a magnetic field of 4-8 Tesla.

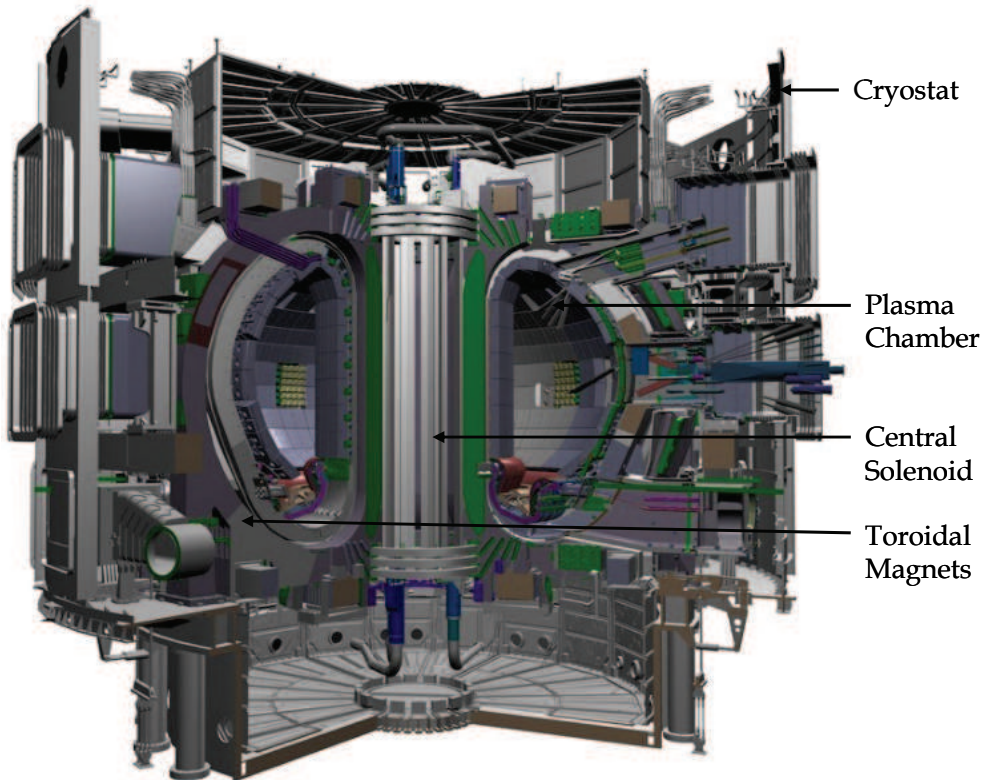


Fig. 20. Details of the TOKOMAK

Tritium breeding modules are used in fusion reactors to produce Tritium by reacting Lithium with neutrons a byproduct of the nuclear fusion reaction. The two basic breeder concepts developed by ITER are liquid breeder and solid breeders. The advantages of liquid breeder over solid breeder are the high Tritium breeding ratio and the Lead-Lithium eutectic can also act as a coolant inside the breeding module which is subjected to high heat

from plasma and the heat generated in itself due to bombardment of neutrons. The major disadvantages of liquid breeders over solid breeders is the pressure drop in the form of Lorentz force and the reduction in convective heat transfer characteristics of the liquid metal when it is flowing in the presence of intense magnetic field produced by the cryogenic super-conducting magnets.

Wong *et al.* (2008) has mentioned about the various liquid metal breeders being developed around the world details of which is given in the table 3. All the liquid breeder design uses Lithium as the breeding material though most of them use a eutectic of Lead and Lithium because of the lower electrical conductivity and the neutron multiplication ability of Lead.

Country	Name of TBM	Liquid Metal Used
US	DCLL - Dual Coolant Lead Lithium	PbLi
EU	HCLL - Helium Cooled Lithium Lead	PbLi
Korea	HCML - Helium Cooled Molten Lithium	Li
India	LLCB - Lead-Lithium Cooled Ceramic Breeder	PbLi
China	DFLL - Dual Functional Lithium Lead	PbLi

Table 3. Details of the liquid TBM developed in the various countries, Wong *et al.* (2008)

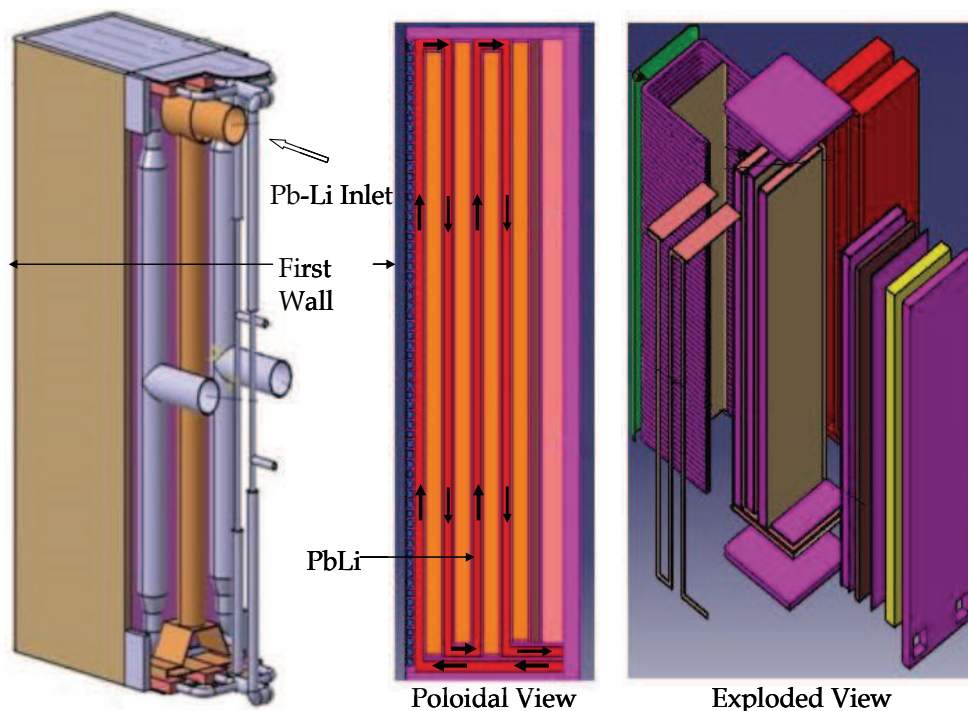


Fig. 21. Details of LLCB- TBM, Wong *et al.* (2008)

Indian Lead lithium Cooled Ceramic Breeder (LLCB) – The design description of LLCB is given in Rao *et al.* (2008). The details of the exploded and cut section views of the LLCB – TBM is shown in figure 21. The two coolants used in LLCB are Helium and a eutectic of Lead-Lithium, Pb-Li. The two coolants are of different molecular properties as Pb-Li has very low Prandtl Number of the order 10^{-2} and Helium gas has Prandtl number of ~ 0.65 . The thermal diffusivity of the two fluids were different as the main temperature difference for Helium in straight ducts were concentrated at the viscous sub layer where as the temperature difference for Pb-Li was also present in the mean core region.

The material of construction of the cooling channels is Ferritic-Martensitic Steel (FMS) having electrical conductivity of the order 10^6 $1/\Omega\text{-m}$, so the pressure drop associated with the flow was very high. Hence a coating of Alumina (Al_2O_3), which has very low electrical conductivity ($\sim 10^{-8}$ $1/\Omega\text{-m}$) is used on the wet surfaces of the cooling channels This makes the configuration similar to the rectangular channel of Shercliff's case with all walls insulating i.e. $d_A = 0$ and $d_B = 0$ and hence as mentioned in 4.2.1, the velocity profiles will not have a high velocity jet near the side walls. So the effect of turbulence modification is more significant on the heat transfer characteristics as mentioned in section 6.2.1. The flow will be electromagnetically laminarized and the heat transfer capacity of the Pb-Li deteriorates at high Hartmann numbers.

9. Nomenclature

$2a$	Distance between Hartmann walls
$2b$	Distance between side walls
B_0	Magnetic field
c	Speed of light
C_p	Specific heat
d_A	Electrical conductivity of wall AA
d_B	Electrical conductivity of wall BB
D	Displacement current
E	Electric field
H	Magnetic field strength
Ha	Hartmann Number
j	Electric charge
k	Thermal conductivity
k_{eff}	Effective thermal conductivity
k_T	Turbulent thermal conductivity
L	Characteristic length
N	Interaction parameter
Nu	Nusselt number
p	Pressure
Pr	Prandtl number
Pr_m	Magnetic Prandtl number
q'''	Volumetric heat generation
S	Source term
Re	Reynolds number

Re_m	Magnetic Reynolds number
t	Time
T	Temperature
U	Axial velocity
U_c	Centre line velocity
U_0	Mean velocity
σ	Electrical conductivity of fluid
η	Non-dimensionalized distance in y direction
ξ	Non-dimensionalized distance in x direction
ν	Kinematic viscosity of fluid
ν_{eff}	Effective viscosity
ν_τ	Turbulent viscosity
ρ	Density of fluid
μ	Dynamic viscosity of fluid
μ^*	Magnetic permeability
ρ_c	Electric charge density

10. Acknowledgement

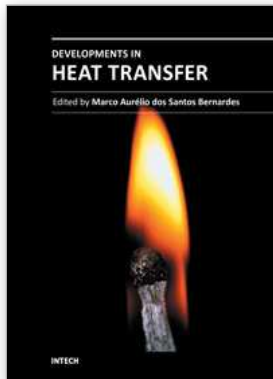
We would like to acknowledge Altair Engineering India Pvt. Ltd., for providing an opportunity to do the associated work

11. References

- Alfven, H. (1942). Existence of electromagnetic-hydrodynamic waves. *Nature*, Vol.150, (1942), pp.405-406.
- Davidson, H. W. (1968). *Compilation of thermo-physical properties of liquid Lithium..* NASA Technical Note, Washington. D. C., 1968.
- Evtushenko, I. A.; Hua, T. Q.; Kirillov, I. R.; Reed, C. B. & Sidorenkov, S. S. (1995). The effect of a magnetic field on heat transfer in a slotted channel. *Journal of Fusion Engineering and Design*, Vol. 27, (1995), pp. 587-592.
- Fink, D. & Beaty, H. W. (October 1999). *Standard handbook for electrical engineers* (14th Edition). McGraw Hill, ISBN 0070220050.
- Gardener, R. A. & Lykoudis, P. S. (1971a). Magneto-fluid-mechanic pipe flow in a transverse magnetic field Part 1 Isothermal flow. *Journal of Fluid Mechanics*, Vol.47, (1971), pp 737-764.
- Gardener, R. A. & Lykoudis, P. S. (1971b). Magneto-fluid-mechanic pipe flow in a transverse magnetic field Part 1 Heat Transfer. *Journal of Fluid Mechanics*, Vol.48, (1971), pp. 129-141.
- Happel, J. & Brenner, H. (1981). *Low Reynolds Number Hydrodynamics*, Springer. ISBN 9001371159.

- Hartmann, J. (1937) Theory of the laminar flow of electrically conductive liquid in a homogeneous magnetic field, *Hg-Dynamics, Kgl. Danske Videnskab. Selskab. Mat.-fus. Medd.*, Vol.15, No.6, (1937)
- Hartmann, J. & Lazarus. P. (1937). Experimental investigation of flow of Mercury in a homogeneous magnetic field, *Kgl. Danske Videnskabernes Selskab, Math.,Fys. Med*, Vol.14, No. 7, (1937).
- Hunt, J. C. R. (1965). Magnetohydrodynamic flow in rectangular ducts. *Journal of fluid mechanics*, Vol. 21, No. 4, (1965), pp. 577-590.
- Hunt, J. C. R. & Stewartson, K. (1965). Magnetohydrodynamic flow in rectangular ducts. II. *Journal of fluid mechanics*, Vol. 23, No.3, (1965), pp. 563-581.
- Ji, H. C. & Gardener, R. A. (1997). Numerical analysis of turbulent pipe flow in a transverse magnetic field. *International Journal of Heat and Mass Transfer*, Vol.40, No.8, (1997), pp. 1839-1851.
- Kirillov, I. R.; Reed, C. B.; Barleon, L. & Miyazaki, K. (1994). Present understanding of MHD and heat transfer phenomenon for liquid metal blankets, *Proceedings of 3rd International Symposium of Fusion Nuclear Technology*, Los Angeles, 1994.
- Lielpeteris, J & Moreau, R. (1989). *Liquid metal magnetohydrodynamics*, Kluwer Academic Publishers Group, ISBN 079230344X, Dordrecht, Boston.
- Luo, X.; Ying, A. & Abodu, M. (2003). Experimental and computational simulation of free jet characteristics under transverse field gradients. *Journal of Fusion Science and Technology*, Vol 44, (July 2003), pp. 85-93.
- Miyazaki, K.; Inoue, h.; Kimoto, T. ; Yamashita, S.; Inoue, S. & Yamaoka, N. (1986). Heat transfer and temperature fluctuation of lithium flowing under transverse magnetic field. *Journal of Nuclear Science and Technology*, Vol.23, (1986), pp. 582-593.
- Miyazaki, K.; Yokomizo, K.; Nakano, M.; Horiba, T. & Inoue, S. *et al.* (1988). Heat Transfer and Pressure Drop of Lithium Flow under Longitudinal Strong Magnetic Field, *Proceedings of LIMET'88, Avignon, 1988.*
- Moffatt, H. K. (1967). On the suppression of turbulence by a uniform magnetic field. *Journal of Fluid Mechanics*, Vol. 28, (1967), pp. 571-592.
- Muller, U. & Buhler, H. (2001), *Magneto-fluid-dynamics in Channels and Containers* (1st Edition), Springer, ISBN 978-3-540-41253-3.
- Rao, J. S. *et al.* (2008). *Design description document for the dual coolant Pb 17Li (DCLL) test blanket module*, Report to the ITER test blanket working group (TBWG), (2008), Institute of Plasma Research, India.
- Rao, J. S. & Sankar, H. (2011). Numerical Simulation of MHD Effects on Convective Heat Transfer Characteristics of Flow of Liquid Metal in Annular Tube. *Journal of Fusion Engineering and Design*, Vol.86, No.2-3, (March 2011), pp. 183-191.
- Roberts, P. H. (1967). *An Introduction to Magnetohydrodynamics*, Longmans Green and Co Ltd, 1967, ISBN 978-0-582-44728-8.
- Shercliff, J. A. (1953). Steady motion of conducting fluids in pipes under transverse magnetic fields, *Proceedings of Cambridge Philosophical Society*, pp. 136-144, 1953.
- Uda, N.; Miyazawa, A. ; Inoue, S.; Yamaoka, n.; Horiike, H. & Miyazaki, k. (2001). Forced convection heat transfer and temperature fluctuations of lithium under

- transverse magnetic field. *Journal of Nuclear Science and Technology*, Vol. 38, (2001), pp. 936-943.
- Uda, N.; Miyazawa, A.; Yamaoka, H. N.; Horiike, H. & Miyazaki, K. (2002). Heat transfer enhancement in lithium annular flow under transverse magnetic field. *Energy Conversion and Management*, Vol.43, (2002), pp. 441-447.
- Wong, C. P. C. ; Salavy, J. F.; Kim, Y.; Kirillov, I.; Kumar, E. R.; Morley, n. B.; Tanaka, S. & Wu, Y. C. (2008). Overview of liquid metal TBM concepts and programs. *Journal of Fusion Engineering and Design*, Vol.83, (2008), pp. 850-857.



Developments in Heat Transfer

Edited by Dr. Marco Aurelio Dos Santos Bernardes

ISBN 978-953-307-569-3

Hard cover, 688 pages

Publisher InTech

Published online 15, September, 2011

Published in print edition September, 2011

This book comprises heat transfer fundamental concepts and modes (specifically conduction, convection and radiation), bioheat, entransy theory development, micro heat transfer, high temperature applications, turbulent shear flows, mass transfer, heat pipes, design optimization, medical therapies, fiber-optics, heat transfer in surfactant solutions, landmine detection, heat exchangers, radiant floor, packed bed thermal storage systems, inverse space marching method, heat transfer in short slot ducts, freezing and drying mechanisms, variable property effects in heat transfer, heat transfer in electronics and process industries, fission-track thermochronology, combustion, heat transfer in liquid metal flows, human comfort in underground mining, heat transfer on electrical discharge machining and mixing convection. The experimental and theoretical investigations, assessment and enhancement techniques illustrated here aspire to be useful for many researchers, scientists, engineers and graduate students.

How to reference

In order to correctly reference this scholarly work, feel free to copy and paste the following:

J. S. Rao and Hari Sankar (2011). Magneto Hydro-Dynamics and Heat Transfer in Liquid Metal Flows, Developments in Heat Transfer, Dr. Marco Aurelio Dos Santos Bernardes (Ed.), ISBN: 978-953-307-569-3, InTech, Available from: <http://www.intechopen.com/books/developments-in-heat-transfer/magneto-hydro-dynamics-and-heat-transfer-in-liquid-metal-flows>

INTECH
open science | open minds

InTech Europe

University Campus STeP Ri
Slavka Krautzeka 83/A
51000 Rijeka, Croatia
Phone: +385 (51) 770 447
Fax: +385 (51) 686 166
www.intechopen.com

InTech China

Unit 405, Office Block, Hotel Equatorial Shanghai
No.65, Yan An Road (West), Shanghai, 200040, China
中国上海市延安西路65号上海国际贵都大饭店办公楼405单元
Phone: +86-21-62489820
Fax: +86-21-62489821

© 2011 The Author(s). Licensee IntechOpen. This chapter is distributed under the terms of the [Creative Commons Attribution-NonCommercial-ShareAlike-3.0 License](#), which permits use, distribution and reproduction for non-commercial purposes, provided the original is properly cited and derivative works building on this content are distributed under the same license.